THE JOURNAL OF PHYSICAL CHEMISTRY C

Article

pubs.acs.org/JPCC

Surface Structure of $V_2O_3(0001)$: A Combined I/V-LEED and STM Study

Felix E. Feiten, Helmut Kuhlenbeck,* and Hans-Joachim Freund

Department of Chemical Physics, Fritz Haber Institute of the Max-Planck Society, Faradayweg 4-6, 14195 Berlin, Germany

Supporting Information

ABSTRACT: Using I/V-LEED and scanning tunneling microscopy, we have investigated the surface structure of ~100 Å thick $V_2O_3(0001)$ films on Au(111). Both methods clearly show that the surface is terminated by a layer of vanadyl groups. I/V-LEED quantitative structure determination applied to differently prepared films always leads to a Pendry *R*-factor for the V═O termination close to 0.11 while the *R*-factor for a reconstructed O_3 termination is always larger than 0.2 and increases with increasing data set size. These results are at variance with a recent publication by Window et al. [*Phys. Rev. Lett.* **2015**, *114*, 216101] in which the authors propose that the $V_2O_3(0001)$ surface is terminated by a reconstructed O_3 structure. Surface oxidation experiments also contradict the conclusions of Window et al. since oxidation leads to a previously identified structure with a $(\sqrt{3} \times \sqrt{3})R30°$ LEED pattern which is not expected for oxidation of an O3-terminated surface. In the course of the I/V-LEED calculations the individual Debye temperatures of the surface atoms were determined as part of the structural optimization procedure. We show that this approach is superior to the kinematical analysis of temperature-dependent LEED measurements.

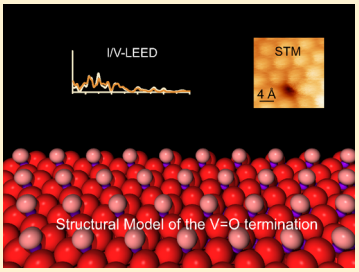

INTRODUCTION

Transition metal oxides play a crucial role in heterogeneous catalysis as support materials for metal nanoparticles, but they also show catalytic activity themselves.[1−4] Knowledge of their atomic scale surface structure is necessary to understand catalytic reactions on them. Vanadium oxides are widely used in industrial oxygen transfer catalysts.[5,6] While phosphorus-doped V_2O_5 is the vanadium oxide most commonly employed in the industry, the $V_2O_3(0001)$ surface also shows catalytic activity.[7,8]

The surface structure is a relevant parameter for catalytic reactions, and therefore the termination of V_2O_3 films prepared in UHV has been discussed in a number of publications.[9−19] Different structural models discussed in these publications are graphically summarized in Figure 1. V_2O_3 crystallizes in the corundum structure. A cut parallel to the 0001 plane can lead to three different surface terminations: a double metal termination (DM) with two vanadium atoms in the surface unit cell, a single metal termination (SM) with one vanadium atom in the surface unit cell, and an oxygen termination (bulk O_3) with three oxygen atoms in the topmost layer. Density functional theory (DFT) calculations[9,10] predict a number of structures to be more stable than these bulk-like terminations: while at very low chemical potentials of oxygen the surface is expected to be vanadium terminated, vanadyl covered surfaces are predicted for higher oxygen potentials. With increasing oxygen pressure the V═O groups are subsequently removed, leading to supercells missing 1/3 or 2/3 of the V═O groups. Both structures exhibit a $(\sqrt{3} \times \sqrt{3})R30°$ superstructure in the LEED pattern and are henceforth called $\sqrt{3}$ structure without differentiating between them. Finally, at even higher oxygen chemical potentials a termination with an oxygen layer at the surface is predicted. In this structure, below the surface every second vanadium atom from the second layer moves up to the first layer to compensate for the charge of the oxygen layer. This is called the reconstructed (rec) O_3 termination.

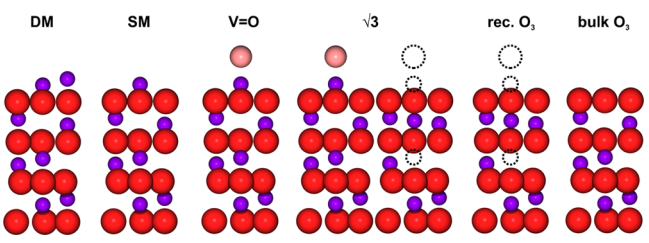

Figure 1. Side-view models of different surface terminations of $V_2O_3(0001)$. Oxygen atoms are depicted in red (pink for V═O oxygen) and vanadium atoms in purple.

For years the accepted view was that the surface is fully covered by vanadyl groups under common UHV conditions. This was based mostly on vibrational spectra (IRAS and HREELS) which show a strong peak for the V═O stretching mode at 127 meV and the fact that atomically resolved STM (scanning tunneling microscopy) images show a simple (1 × 1) pattern similar to what is expected for a vanadyl-terminated surface.[11,12] NEXAFS (near-edge X-ray absorption fine structure) and XPS (X-ray photoelectron spectroscopy) spectra also fit to a V═O-terminated surface.[13] On the other hand, several ion scattering studies favor the reconstructed O_3 termination.[14−16] In a recent publication we have shown, by

Received: July 17, 2015
Revised: September 4, 2015
Published: September 11, 2015

DOI: 10.1021/acs.jpcc.5b06943
J. Phys. Chem. C 2015, 119, 22961−22969

using I/V-LEED (I/V analysis of LEED [low-energy electron diffraction]), STM, ion scattering, and DFT that the surface is most likely vanadyl terminated.[17]

In this paper we combine STM with I/V-LEED to investigate the V_2O_3 surface structure. Scanning tunneling microscopy can give atomically resolved structural information, but contrary to I/V-LEED, there is no chemical sensitivity to identify the types of atoms and STM does only supply information about the very surface. On the other hand, STM can give quickly (if the tip performs well) an impression of the quality of the film, revealing the types and the density of the defects. Deviations from the ideal surface structure like defect structures, shear planes, stacking faults,[20] etc., or more or less ordered contamination layers may influence experimental I/V curves and thus impair the results of I/V LEED studies. Therefore, the role of STM in such a quantitative LEED experiment may be the control and the optimization of the surface quality. I/V-LEED can be applied best to well-ordered systems, and STM can help to establish such systems and to verify that they are well-ordered.

We have also determined surface Debye temperatures by using them as parameters in the I/V-LEED calculations. Finally, we discuss our results in the context of previous publications on the $V_2O_3(0001)$ surface.

EXPERIMENTAL DETAILS

Experiments were conducted in an Omicron UHV chamber with a background pressure $<5 \times 10^{-11}$ mbar. The chamber is equipped with a room temperature STM (STM-1) and a MCP LEED system as well as an X-ray source with Al and Mg anodes and a hemispherical analyzer for XPS, all from Omicron. Sample cleaning is done via Ar^+ ion bombardment and annealing with a W filament behind the sample. An Au(111) crystal, bought from MaTeck, Germany, was used as substrate for the growth of the $V_2O_3(0001)$ film. The sample temperature was measured with a K-type thermocouple, spot-welded to two Mo plates which fix the crystal on the sample holder. Prior to film deposition the cleanliness and surface ordering of the Au crystal were checked by XPS, LEED, and STM.

Vanadium was deposited in an oxygen atmosphere with an Omicron EFM-3T evaporator at a rate of about 0.7 Å/min, as determined by calibration with a quartz crystal microbalance. Oxygen pressure and sample temperature during vanadium deposition were varied between 523 and 670 K and between 1×10^{-7} and 2×10^{-6} mbar of O_2 for different preparations. Typically 5.4 nm of V, corresponding to 10 nm of V_2O_3, was deposited. After deposition the films were first annealed in O_2 with the same oxygen pressure as during deposition, followed by an annealing step at increased temperature in UHV to improve the order of the film.

While the oxygen pressure was set via filling the whole chamber with O_2 during film deposition, a custom-built pinhole doser was used to generate pressures up to 6×10^{-5} mbar at the sample surface in postannealing steps. Details of the preparation of the samples discussed in this publication can be found in Table 1. In this table the steps B to G for film 3 as well as B to M and Q to S for film 4 are omitted since those preparations are not discussed here. They can be found in the Supporting Information, Table S1.

I/V-LEED quantitative structure determination works best if the electron incidence direction differs from the sample normal by not more than a few tenths of a degree. In order to achieve this condition, one Helmholtz coil was mounted at the chamber.[21] Varying the magnetic field strength by adjusting the current running through the coil as a function of the electron beam energy allows for simultaneous compensation of the magnetic field at the sample position and the correction of small angular sample misalignments. We only employed one coil because a measurement of the magnetic field strength at the sample position showed that only the vertical component was significant (40−50 μT) while the magnetic field in the horizontal directions was very small ($\approx$1 μT). A Sony black and white digital camera was used to take images of the LEED screen; typical exposure times were between 300 and 500 ms per image.

The current of the electron beam to the sample was less than 10 nA in the I/V-LEED experiments. A very slight difference between subsequently recorded I/V curves was recognizable under this condition, which we attribute to a slight oxygen depletion. A clear effect of this reduction on the *R*-factor could not be detected. For testing purposes also some I/V curves with a significantly reduced ion flux were measured. In this case no effect of the electron irradiation could be detected, and the

Table 1. Details of Some Preparation Steps for the Films Discussed in This Work

no.	step	preparation details	LEED pattern/comment
1	A	film deposition: 650 K, 2.5×10^{-7} mbar O_2	
		annealing: 700 K, 3×10^{-7} mbar O_2, 20 min	(1 × 1)
		annealing: 800 K, 5×10^{-9} mbar, 10 min	
	B	annealing: 870 K, 5×10^{-8} mbar O_2, 10 min	(1 × 1)
	C	annealing: 870 K, 5×10^{-6} mbar O_2, 15 min	$\sqrt{3}$
	D	annealing: 870 K, 6×10^{-5} mbar O_2, 15 min	formation of V_2O_5 and evaporation
2	A	film deposition: 600 K, 1×10^{-7} mbar O_2	
		annealing: 650 K, 1×10^{-7} mbar O_2, 15 min	(1 × 1)
		annealing: 870 K, 1.6×10^{-9} mbar, 10 min	
	B	annealing: 850 K, 1.1×10^{-10} mbar, 30 min	(1 × 1)
3	A	film deposition: 523 K, 2×10^{-7} mbar O_2	(1 × 1)
		annealing: 523 K, 2×10^{-7} mbar O_2, 15 min	
		...	
	H	annealing: 900 K, 2.9×10^{-10} mbar, 30 min	(1 × 1)
	I	annealing: 900 K, 5×10^{-7} mbar O_2, 60 min	(1 × 1)
	J	annealing: 900 K, 5×10^{-7} mbar O_2, 150 min	(1 × 1)
4	A	film deposition: 573 K, 2×10^{-6} mbar O_2	$\sqrt{3}$
		annealing: 773 K, 2×10^{-6} mbar O_2, 15 min	
		...	
	N	annealing: 950 K, 2×10^{-7} mbar O_2, 105 min	(1 × 1)
	O	annealing: 923 K, 1.3×10^{-10} mbar, 23 min	(1 × 1)
	P	XPS measurements for 4 h	(1 × 1)
		...	

DOI: 10.1021/acs.jpcc.5b06943
J. Phys. Chem. C 2015, 119, 22961−22969

curves were essentially identical to the ones measured with higher electron currents.

Two correction functions to the experimental I/V curves were measured, and the data were corrected accordingly: First, the current of the primary beam depends on the beam energy E_{beam}. This current was determined by measuring the current of electrons flowing from the sample to ground with the sample set to a positive bias voltage in order to limit the contribution of secondary electrons. Second, the MCP detection sensitivity varies with E_{beam} since the electron impact energy at the MCP varies with E_{beam}. This dependence was measured through variation of the front bias of the MCP for a constant beam energy.

COMPUTATIONAL DETAILS

I/V curves were calculated using a modified version of the SATLEED package by A. Barbieri and M. A. van Hove (available for download at http://www.icts.hkbu.edu.hk/vanhove/). Fourteen different trial structures were used as starting structures in the optimization runs: five single metal (SM), two double metal (DM), five vanadyl (VO), and two reconstructed O_3 (O3) terminations, based on structures published in a number of theoretical and experimental publications on the $V_2O_3(0001)$ surface.[9,15,18,22,23] Different models of the same type, e.g., two different VO structures, have different interlayer distances. A table with structural details for all starting structures can be found in the Supporting Information, Table S2. We used an evolutionary strategy algorithm (CMA-ES) to optimize the trial structures by minimization of the Pendry *R*-factor.[24] In the optimization runs the coordinates of all atoms above the fourth O_3 layer below the surface were varied in order to minimize the *R*-factor (see Figure 8). Thus, 15−17 atomic coordinates were optimized depending on the structural model: 15 coordinates for the O3 models, 16 coordinates for the SM models, and 17 coordinates for the VO and DM models. The C_3 symmetry of the system couples the coordinates of the three oxygen atoms in the 2d unit cell in each layer so that only the coordinates of one of these atoms had to be optimized. The vanadium atoms are located on C_3 axes. In this case such a coupling does not exist, but the atom coordinates in the surface plane were not varied in order to not violate the C_3 symmetry. Other optimization parameters were three to five Debye temperatures characterizing the vibrational amplitudes of the atoms, the real and imaginary parts of the inner potential, a linear background, and the in-plane lattice parameter *a*. The five Debye temperatures T_{Debye} are those of the bulk vanadium and oxygen atoms, that of the oxygen atoms in top O_3 layer, that of topmost V atoms in V═O and metal terminations, and that of the O atoms in the vanadyl groups. The structural optimizations runs were started with the highest angular momentum number considered in the calculations set to LMAX = 7 and a 2 eV electron energy step width, followed by another full optimization using the parameters resulting from the first step as start configuration but LMAX = 9 and 1 eV steps. The relativistic phase shifts employed were calculated for bulk V_2O_3 using the phase shift program that comes with the SATLEED package.

RESULTS

As we have shown previously, oxidation of the as-prepared films with a (1 × 1) hexagonal LEED pattern leads to a $\sqrt{3}$ structure followed by the formation of V_2O_5 which sublimates at sufficiently high temperature. This is a first hint that the surface is not terminated by a reconstructed O3 layer since the oxygen content in the O3 structure is higher than in the $\sqrt{3}$ structure if we accept the structural models of the $(\sqrt{3} \times \sqrt{3})R30°$ structure published in refs 9 and 10. Therefore, oxidation of the O3 structure should not lead to a $\sqrt{3}$ structure. LEED patterns observed after different preparation treatments of film no. 1 are shown in Figure 2.[17]

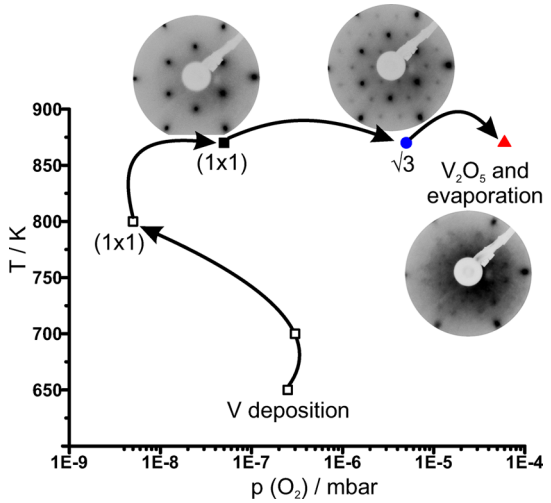

Figure 2. Preparation steps of film no. 1. At some points characteristic LEED patterns (electron energy = 100 eV) are shown.

While V_2O_5 was not directly observed, its formation and evaporation were concluded from the observation that in the oxidation experiment the V_2O_3 LEED pattern disappeared and the Au (substrate) peaks in XPS increased significantly (Figure S1). While V_2O_3 is thermally stable in UHV up to <1000 K, V_2O_5 begins to sublimate in UHV at 823 K.[25]

STM. STM images of the (1 × 1) structure show a honeycomb lattice with two different types of defects. Dark depressions correspond to missing vanadyl groups while bright triangular features are attributed to the reduction of the surface since they can be observed after irradiating the sample with electrons. The type and the density of surface defects depend on the preparation conditions. Figure 3A shows the trimeric features of a reduced surface for film no. 3. Annealing this sample in oxygen led to their disappearance and the appearance of dark depressions (Figure 3B). Further oxidation increased the density of dark depressions (Figure 3C). The LEED patterns of these three surfaces are essentially indistinguishable by visual inspection, and only by STM is it possible to identify these structures, which permits to take specific measures to remove them.

I/V-LEED Symmetry. Two schematic drawings of the V_2O_3 LEED pattern are shown in Figure 4. Figure 4A shows the LEED patterns of $V_2O_3(0001)$ (black circles) and Au(111) (gray stars). The $V_2O_3(0001)$ surface has C_3 symmetry, and thus the six diffraction spots surrounding the (0 0) reflex should consist of two sets of symmetry inequivalent beams. In reality, however, the experimental I/V curves of all six spots appear to be identical. This is due to mirror planes in the Au(111) substrate shown as gray dashed lines in Figure 4A. They are responsible for the presence of two different domains in the V_2O_3 film, related to each other through a mirror operation.

DOI: 10.1021/acs.jpcc.5b06943
J. Phys. Chem. C 2015, 119, 22961−22969

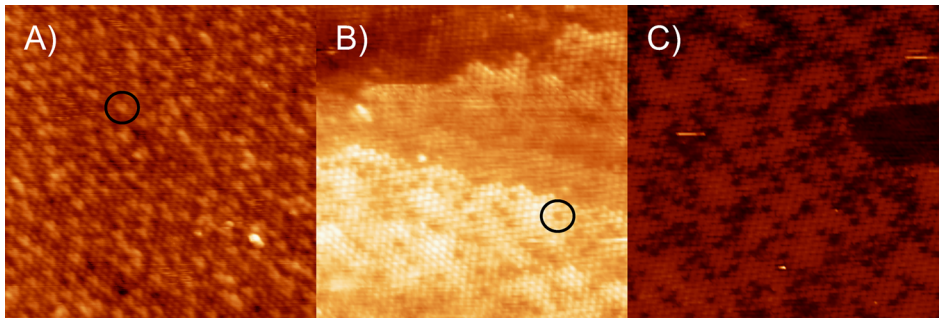

Figure 3. STM images illustrating the oxidation of slightly substoichiometric $V_2O_3(0001)$. 20 nm × 20 nm, +1 V, 0.1 nA. All images are from film no. 3. (A) Preparation step H, reduced surface. (B) Step I, trimeric features gone. (C) Step J, number of missing V═O groups increased. One of each of the two types of defects is encircled in (A) and (B), respectively. See Table 1 for details of the preparation steps.

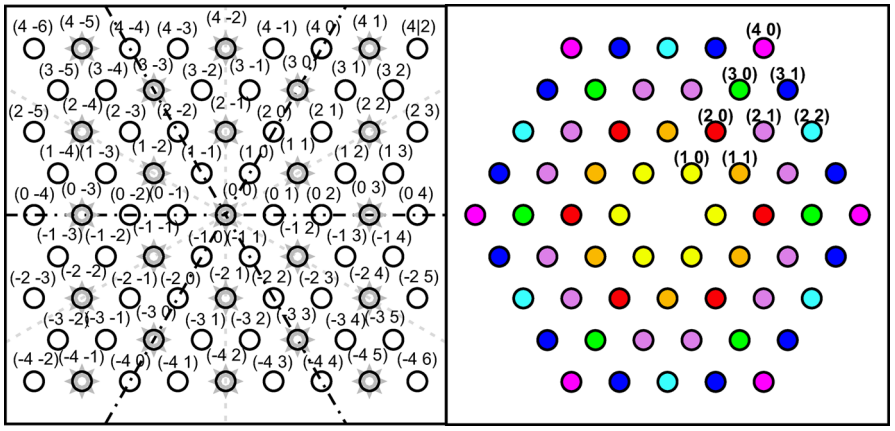

Figure 4. (A) Scheme of the $V_2O_3(0001)$ (black circles) and Au(111) (gray stars) LEED patterns with lines of apparent symmetry as explained in the text. (B) Color-coded scheme showing spots with similar I/V curves in the same color.

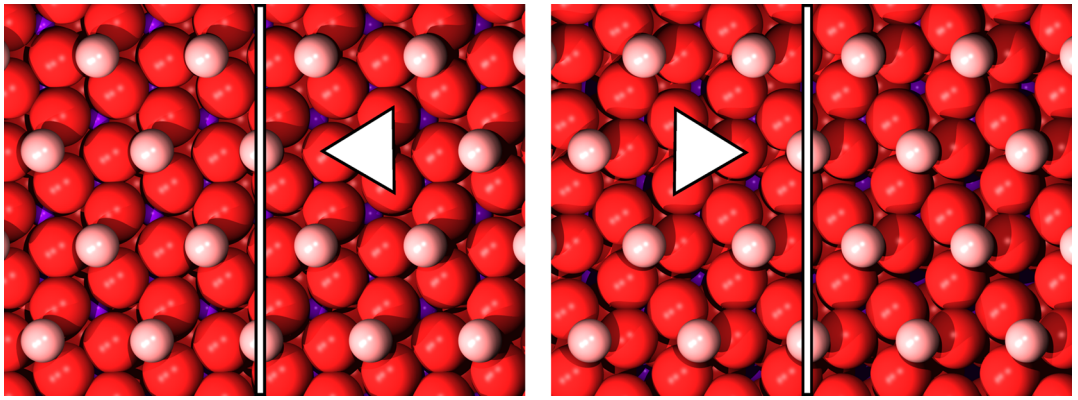

Figure 5. Models of two subsequent vanadyl-terminated surfaces. Oxygen trimers and the mirror plane which transforms them into each other are indicated.

The LEED intensities corresponding to these two domains add up in the LEED pattern, and equal abundance of both domains leads to the observed quasi-6-fold symmetry. This explains the equivalent I/V curves for many of the diffraction spots which are not symmetry-equivalent in C_3, but not for all of them, like the (1 1) and the (−1 2) spots. The identical intensities of these spots are related to the different azimuthal orientations of the oxygen trimers in subsequent layers of the V_2O_3 structure. Figure 5 shows surfaces of two subsequent oxygen layers with vanadyl groups on top. The oxygen layers have a slightly distorted hexagonal structure and can be constructed from the oxygen trimers indicated by triangles. These two surfaces can be transformed into each other by a mirror operation using the mirror plane indicated as a vertical line in Figure 5 plus a translation. Equal abundance (which is quite likely the case) of both types of surface leads to lines of effective symmetry in the LEED pattern, indicated as black dash-dotted lines in Figure 4A. The resulting apparent symmetry of the V_2O_3 LEED pattern is shown in Figure 4B where diffraction spots with identical I/V curves have the same color. We note that the equal abundance of domains related to the Au(111) mirror planes cannot be taken for granted. A miscut of the Au(111) surface may break the mirror symmetry and influence the abundance of the $V_2O_3(0001)$ domains. However, in our

DOI: 10.1021/acs.jpcc.5b06943
J. Phys. Chem. C 2015, 119, 22961−22969

experiments we always found the effective symmetry indicated in Figure 4B.

Debye Temperature Determination. Atomic vibrations influence the diffraction of electrons and have to be considered in I/V-LEED calculations. They are usually described through the Debye temperature Θ_D within the Debye model. In I/V-LEED, instead of the bulk Debye temperature $\Theta_{D,bulk}$, the surface Debye temperature $\Theta_{D,surf}$ is used in order to take into account the different vibrational properties of surface atoms. Van Delft has shown that surface Debye temperatures $\Theta_{D,surf}$ can be roughly estimated by multiplying $\Theta_{D,bulk}$ with $1/\sqrt{2}$.[26] Using a bulk Debye temperature of 580 K for V_2O_3[27] gives $\Theta_{D,surf} \approx 410$ K.

Temperature-dependent measurements of LEED intensities allow the experimental determination of $\Theta_{D,surf}$ as shown by Jepsen and Marcus.[28] As these authors have shown themselves, this method is relatively inaccurate. In our case this procedure is further complicated since it involves an effective mass which is hard to define for systems containing more than one sort of atoms.[29] Furthermore, this approach yields only a single value for $\Theta_{D,surf}$. However, inequivalent surface atoms will have different vibrational properties, and therefore their Debye temperatures will in general be different. The vibrational amplitudes of the atoms (and therefore their Debye temperatures) are relevant input parameters for I/V-LEED computations, and therefore we decided not to use a probably inaccurate Debye temperature $\Theta_{D,surf}$ determined with the method mentioned above, but instead to use the Debye temperatures of the atoms in the model structures as parameters in the optimization runs as described in the Computational Details section. Table 2 gives an overview of the temperatures obtained in this way with the I/V-LEED calculations discussed later in this text. The Debye temperatures for O and V atoms in the vanadyl groups are always smaller than the Debye temperatures of deeper lying atoms, as expected. Together with the Debye temperature for the top O3 layer they are close to the surface Debye temperature of 410 K estimated with the $\Theta_{D,surf} \approx 1/\sqrt{2}\Theta_{D,bulk}$ rule. The values for lower lying atoms, labeled "bulk" in Table 2, closely match the bulk Debye temperature of 580 K. The good agreement between the bulk values listed in Table 2 and the literature bulk value indicates that this method delivers reasonably accurate values. The spread of the values for different preparations in Table 2 may give an impression of the accuracy of the Debye temperatures determined with I/V-LEED.

Table 2. Debye Temperatures Θ_D Determined with I/V-LEED Optimization Runs, Assuming a Vanadyl-Terminated Surface (Values Listed for Samples #2B, #3H, and #4O)

	Θ_D (K)		
type of atom[a]	exp #2B	exp #3H	exp #4O
vanadyl O	305	315	310
vanadyl V	364	288	366
top O_3 layer O	440	457	443
bulk V	553	596	560
bulk O	631	615	626

[a]"Bulk" refers to all atoms below the topmost O3 layer.

I/V-LEED and STM Measurements. I/V-LEED measurements were always combined with STM in order to document the surface quality before I/V-LEED data were recorded. The STM images in Figure 6 show a surface with missing V═O groups (Figure 6A, sample #2B, taken before I/V-LEED), a somewhat reduced surface with many trimeric features (Figure 6B, sample #3H, taken before I/V-LEED), and a surface with fewer trimeric defects (Figure 6C, #4O, taken after I/V-LEED). I/V-LEED structural optimization as described above was performed for all three of these preparations; the best-fit Pendry *R*-factors are listed in Table 3, and the experimental I/V curves are plotted in Figure 7 together with the curves calculated for the best-fit V═O terminated structure. The Pendry *R*-factors for structural models with double metal (DM) termination were always so large that they are not discussed here.

Table 3. Best-Fit *R*-Factors for Three Preparations and Three Models and the Respective Energy Ranges of the I/V-LEED Measurements

preparation	R_{pendry} (V═O)	R_{pendry} (O3)	R_{pendry} (SM)	total energy range (eV)
#2B	0.12	0.23	0.20	766
#3H	0.10	0.26	0.14	1128
#4O	0.12	0.36	0.23	1819

The energy ranges of the LEED measurements were 50 eV → 300 eV for preparation #2B, 50 eV → 400 eV for preparation #3H, and 50 eV → 500 eV for preparation #4O. This leads to the tabulated total energy ranges as the sum of the energy ranges of symmetry inequivalent spots listed in Table 3. The smallest *R*-factor for all three preparations is the *R*-factor for models with vanadyl termination, which is a clear hint that the $V_2O_3(0001)$ surface is in fact vanadyl terminated. Another indication comes from the dependence of the *R*-factor on the

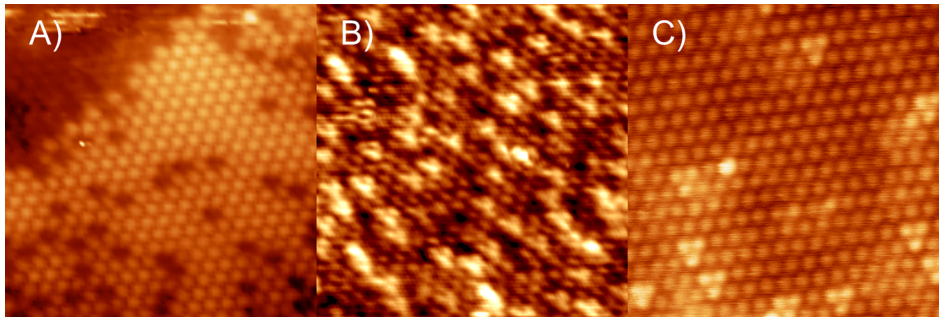

Figure 6. Atomically resolved STM images of different $V_2O_3(0001)$ films: (A) film #2B, taken before I/V-LEED; (B) film #3H, taken before I/V-LEED; (C) film #4O, taken after I/V-LEED. All images 10 nm × 10 nm, +1 V, 0.1 nA.

DOI: 10.1021/acs.jpcc.5b06943
J. Phys. Chem. C 2015, 119, 22961−22969

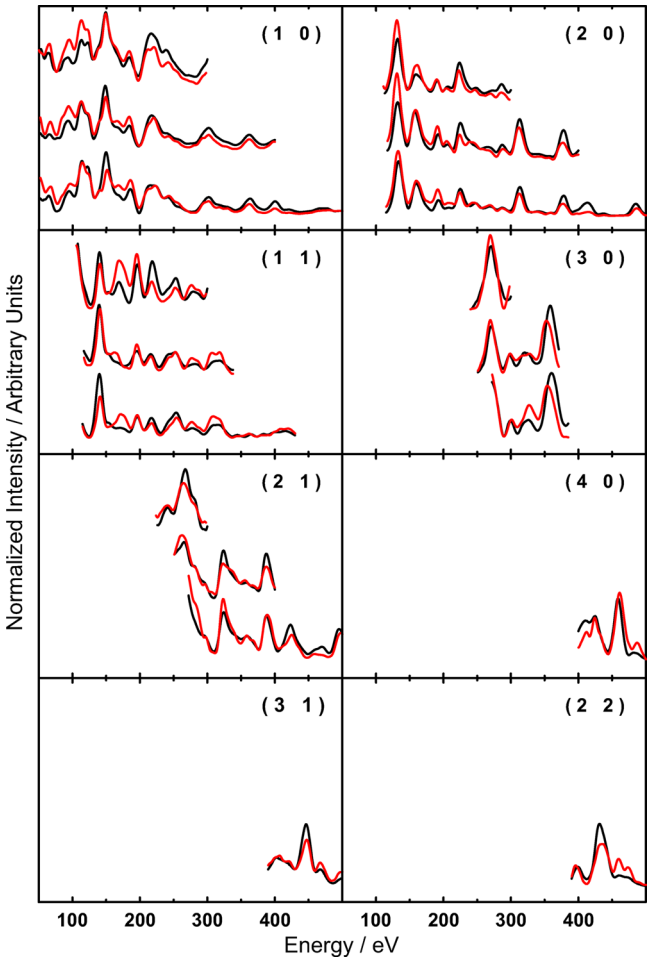

Figure 7. Experimental (black) and computed best-fit (red) I/V curves for a structural model with V═O termination. In each graph the top curves correspond to preparation #2B, the middle curves to preparation #3H, and the bottom curves to preparation #4O.

energy range: the *R*-factors for the models with vanadyl termination do essentially not depend on the energy range, as expected for the correct model, while for the O3 termination the *R*-factor increases with increasing energy range due to the well-known problem of fitting a data set with the wrong function. This may work satisfactorily for a small fit range, but the error will unavoidably increase when the fit range is increased.

We note that the *R*-factors for the SM model are always smaller than those for the O3 model but larger than those for the VO model. This is likely related to the similarity of the VO model and the SM model which differ just by the presence/absence of the vanadyl oxygen atoms, which are comparably weak scatterers, while the structural difference between the VO model and the O3 model is larger (absence of vanadyl groups in the O3 model and upward movement of vanadium atoms below the surface). Best-fit structural parameters for preparation #4O are given in Table S3 for all 14 models tested.

While the I/V-LEED calculations discussed above have been performed with the bulk in plane lattice constant of a = 4.9570 Å,[23] we have also performed calculations for different values of a using the data set of preparation #4O. This lead to a very slight improvement of the *R*-factor to 0.11 for a lattice constant of a = 4.9756 Å. The very small difference of 0.4% between the best-fit lattice constant and the value reported in the literature is another indicator that the V═O structure is the correct model.

The parameters for this structure are tabulated in Table 4 with the corresponding distances visualized in Figure 8. A graph showing the dependence of the *R*-factor on the lattice parameter can be found in Figure S2.

Table 4. Best-Fit Structural Data for Preparation #4O[a]

	VO model	SM model	O3 model
V═O	1.46		
$O3_1$–V	0.61	0.96	
$O3_1$ rotation	+3.5°	+0.2°	+6.2°
$O3_1$ scaling	+1%	−15%	+6%
V_{1A}–$O3_1$	0.98	0.91	0.93
V_{1B}–V_{1A}	0.26	0.29	0.01
V_{1C}–V_{1B}			0.28
$O3_2$–$V_{1B(C)}$	1.06	1.10	1.09
$O3_2$ rotation	+2.4°	+4.3°	+9.2°
$O3_2$ scaling	+3%	+9%	±0%
$V_{2(A)}$–$O3_2$	1.00	0.96	1.35
V_{2B}–V_{2A}	0.39	0.36	
$O3_3$–$V_{2(B)}$	0.99	0.98	0.97
$O3_3$ rotation	−2.0°	0.3°	−6.2°
$O3_3$ scaling	+6%	+9%	−1%
V_{3A}–$O3_3$	0.95	0.98	0.96
V_{3B}–V_{3A}	0.39	0.37	0.29
$O3_4$–V_{3B}	0.95	0.92	1.08

[a]Structural data (layer distances in Å, scaling and rotation of the oxygen trimers) for the VO model using the optimized lattice constant a = 4.9756 Å and for the SM and O_3 models using the bulk value a = 4.9570 Å. Oxygen trimer (O_3) clockwise rotation and scaling are given relative to the bulk values.

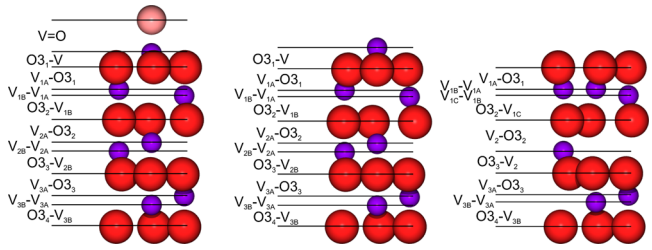

Figure 8. Structural models of the best-fit structures for VO, SM, and O3 termination models using I/V-LEED data for preparation #4O. The corresponding structural data are collected in Table 4.

Comparison of the layer distances in the best-fit V═O terminated structure with those of the bulk structure reveals a decrease of the $O3_1$–V distance by 38%. The next interlayer distance V_{1A}–$O3_1$ is identical to the bulk value of 0.98 Å while the following V_{1B}–V_{1A} distance is again reduced (by 28% compared to the bulk value of 0.36 Å). The remaining changes of interlayer distances are listed in Table S4. They are all smaller than 10%. The changes of the lateral positions of the oxygen atoms compared to the bulk values are rather small for the V═O-terminated model (trimer rotations of 3.5°, 2.4°, and 2.0° and trimer size changes of +1%, +3%, and +6% for the first, second, and third O_3 layer, respectively). The size changes in the best-fit SM struture are significantly larger (−15%, +9%, and +9%, respectively) while the best-fit O3 structure involves much larger rotations (6° and 9°) for the first two O_3 layers.

DOI: 10.1021/acs.jpcc.5b06943
J. Phys. Chem. C 2015, 119, 22961−22969

While the V=O bond length determined here with I/V-LEED (1.46 Å) is slightly shorter than that determined with DFT (1.59, 1.61, and 1.57 Å, respectively),[9,17,19] the changes in interlayer distances resulting from structural optimization in the DFT calculations of Kresse et al.[9] and Feiten et al.[17] match the values determined with I/V-LEED remarkably well as shown by the numbers in Table 5.

Table 5. Comparison of Interlayer Relaxations (in %) Determined with I/V-LEED and DFT[a]

	this study	DFT (PW91)[9]	DFT (HSE)[17]
$O3_1$–V	−38	−31	−34
V_{1A}–$O3_1$	±0	+1	−1
V_{1B}–V_{1A}	−28	−25	−25
$O3_2$–V_{1B}	+8	+10	+9

[a]The changes given are given relative to the corresponding bulk distances. $O3–V_{bulk}$ = 0.98 Å and $V–V_{bulk}$ = 0.36 Å.[23]

A large contraction of the $O3_1$–M distance between the topmost metal atom and the underlying O3 layer has also been found for other oxides with corundum structure, both experimentally (Cr_2O_3[30] and Fe_2O_3[31,32]) and theoretically (Cr_2O_3,[33] Fe_2O_3[34,35]).

DISCUSSION

Our results are in marked contrast to the results of ion scattering studies performed by Window et al., who have found their ion scattering data (medium energy ion scattering (MEIS) and noble gas impact-collision ion scattering spectroscopy (NICISS) data) to be in clear favor of a reconstructed O_3 termination.[15,16] While we cannot explain this discrepancy for the MEIS experiment, the rather thin films (~25 Å compared to ≥100 Å in our studies as well as in the studies using MEIS) and the different substrate ($Cu_3Au(100)$) in the NICISS experiment could be responsible for a different surface termination. This could also be the reason for the unusual STM images obtained by Niehus et al. which they attribute to "a full vanadium layer stabilized by one-third of an oxygen layer".[36]

Window et al. have performed Tersoff–Hamann STM simulations for a V=O-terminated V_2O_3 surface as well as for both bulk-like and reconstructed O3-terminated surfaces (see Figure 1 for the structures). While the simulated STM images of Window et al.[15] show more fine structure for the two O3 terminations than the STM simulations of Surnev et al.,[37] both studies predict round shapes for vanadyl-terminated surfaces and triangular features for O3 terminations. The triangular features observed in our STM images can clearly be attributed to reduction and do not correspond to the O3 model. We have never observed any STM images similar to the simulated STM images for O3-terminated structures. Although the defects that we observe in STM images sometimes do display local order, we have never seen extended ordered areas that could be related to a different coexisting surface structure, which renders the model of coexisting O3 and V=O surface phases as proposed by Window et al.[16] unlikely. Coexisting surface structures, which might be interpreted as arising from differently terminated regions on the surface, have been observed by Surnev et al.[37] Their occurrence could be due to the relatively low thickness of the films investigated (3 monolayer equivalents on Pd(111)).

A quantitative surface structure determination of $V_2O_3(0001)$ using photoelectron diffraction was in favor of a single metal terminated structure but could not exclude the presence of oxygen atoms atop of the V atoms, i.e., V=O groups.[18] While the overall conclusion is in good agreement with our findings, our data clearly favor a vanadyl termination over a single metal terminated structure without oxygen atoms atop. By including the Debye temperatures of the surface atoms in the optimization process, we feel that we have adequately treated vibrational amplitudes within the I/V-LEED calculations, an issue that was raised in the comparison of photoelectron diffraction results with I/V-LEED results for $Al_2O_3(0001)$[38] and $Cr_2O_3(0001)$.[30]

Another ion scattering method, ion beam triangulation (IBT), has also been employed to study the structure of the $V_2O_3(0001)$ surface.[14] The authors came to the conclusion that the surface should be terminated by an O_3 layer. IBT was assumed to be very surface sensitive, but recently it has been shown that this may not be as true as formerly assumed.[39] In the case of $V_2O_3(0001)$ an O3 plane is located below the vanadyl groups, which may be the reason for the results of the IBT study if the contribution of the surface vanadyl groups to the measured signal is less dominant than previously assumed. A different ion scattering experiment, fast atom diffraction, performed on $V_2O_3(0001)$ by the same group strongly supports the conclusion that $V_2O_3(0001)$ is vanadyl terminated, as we have reported recently.[17]

Two DFT studies have predicted phase diagrams for the surface structure of $V_2O_3(0001)$ as a function of the chemical potential of oxygen in the gas phase above the oxide. While Kresse et al. have performed calculations on V_2O_3 slabs,[9] Todorova et al. have considered thin films of V_2O_3 supported on Al_2O_3.[10] Both studies predict the existence of a surface covered by vanadyl groups, which are gradually removed with increasing oxygen chemical potential leading to partially V=O covered surfaces and finally to a reconstructed O3 termination. The stability ranges for different surface terminations reported in refs 9 and 10 indicate that the thermodynamically stable structure is an O3-terminated surface at the typical oxygen pressures and temperatures used in the preparation of the $V_2O_3(0001)$ films. Also, neither of the studies predicts full V=O coverage to be the most stable surface structure at any oxygen chemical potential, rather they favor partial V=O coverage over a range of conditions. However, we note that the GGA and PW91 functionals employed in those studies overestimate the stability of phases with a high oxygen content. Furthermore, the authors of both theoretical studies clearly stated that DFT calculations with semilocal functionals have problems to describe V_2O_3. In particular, the $V_2O_3(0001)$ surface became a ferromagnetic insulator if spin polarization was considered in the DFT calculations, which is in stark contrast with the experimental observation that it is paramagnetic and metallic. We have recently performed DFT calculations using a hybrid functional which appears to describe V_2O_3 more accurately than the functionals previously employed.[17] This is reflected in the better reproduction of the experimental heats of formation of various V_xO_y species. In these calculations the range of the oxygen chemical potential in which the vanadyl-covered surface is predicted to be thermodynamically stable is significantly enlarged compared to earlier DFT studies and the region where an O3-terminated structure is thermodynamically stable corresponds to conditions where V_2O_5 is the stable bulk phase. This explains well

DOI: 10.1021/acs.jpcc.5b06943
J. Phys. Chem. C 2015, 119, 22961–22969

why the O3 structure could not be prepared in this study since V_2O_5 formation prevented the formation of the O3 structure.

CONCLUSION

Our combined I/V-LEED and STM measurements clearly indicate that the $V_2O_3(0001)$ surface is covered by vanadyl groups under typical UHV preparation conditions. This is in marked contrast to conclusions derived from ion scattering experiments by Window et al.[15,16] While the surface could be oxidized to show a $(\sqrt{3} \times \sqrt{3})R30°$ LEED pattern indicative of one of the $\sqrt{3}$ structures, we were not able to prepare an O_3 terminated surface due to the formation and sublimation of V_2O_5 at the required preparation conditions. Through atomically resolved STM images we could distinguish two different types of surface defects. While the surfaces are never completely free of defects, the number of defects could be reduced by annealing in UHV or in an oxygen atmosphere depending on the type of the defects.

We have determined surface Debye temperatures for $V_2O_3(0001)$ by using them as fit parameters in the structural optimizations of the I/V-LEED calculations. This method avoids the shortcomings of the kinematical determination through temperature-dependent measurements of the LEED intensity. Using five different Debye temperatures, we obtained values of $\Theta_{D,surf} \approx 300$ K for the atoms in vanadyl groups, $\Theta_{D,surf} \approx 400$ K for the top oxygen trilayer and $\Theta_{D,bulk} \approx 600$ K for the bulk. The good agreement with the literature value of $\Theta_{D,bulk} = 580$ K[27] indicates the reliability of this method.

ASSOCIATED CONTENT

Supporting Information

The Supporting Information is available free of charge on the ACS Publications website at DOI: 10.1021/acs.jpcc.5b06943.

Preparative details for additional preparation steps; structural data for the start structures used in the I/V-LEED calculations; XPS spectrum indicating V_2O_5 evaporation; structural parameters for best fits resulting from all 14 start structures for preparation #4O; graph showing the dependence of the *R*-factor on the lattice parameter *a*; comparison of interlayer distances (PDF)

AUTHOR INFORMATION

Corresponding Author

*E-mail: kuhlenbeck@fhi-berlin.mpg.de (H.K.).

Notes

The authors declare no competing financial interest.

ACKNOWLEDGMENTS

This work was funded by the Deutsche Forschungsgemeinschaft through their Sonderforschungsbereich 546 "Transition Metal Oxide Aggregates". We gratefully acknowledge the Fonds der Chemischen Industrie for financial support. The LEED calculations were performed using programs derived from the Barbieri/Van Hove Symmetrized Automated LEED package.

REFERENCES

(1) Cuenya, B. R. Synthesis and Catalytic Properties of Metal Nanoparticles: Size, Shape, Support, Composition, and Oxidation State Effects. *Thin Solid Films* **2010**, *518*, 3127−3150.

(2) Freund, H.-J.; Pacchioni, G. Oxide Ultra-Thin Films on Metals: New Materials for the Design of Supported Metal Catalysts. *Chem. Soc. Rev.* **2008**, *37*, 2224−2242.

(3) Royer, S.; Duprez, D. Catalytic Oxidation of Carbon Monoxide over Transition Metal Oxides. *ChemCatChem* **2011**, *3*, 24−65.

(4) Kuhlenbeck, H.; Shaikhutdinov, S.; Freund, H.-J. Well-Ordered Transition Metal Oxide Layers in Model Catalysis - a Series of Case Studies. *Chem. Rev.* **2013**, *113*, 3986−4034.

(5) Wachs, I. E.; Weckhuysen, B. M. Structure and Reactivity of Surface Vanadium Oxide Species on Oxide Supports. *Appl. Catal., A* **1997**, *157*, 67−90.

(6) Haber, J. Fifty Years of my Romance with Vanadium Oxide Catalysts. *Catal. Today* **2009**, *142*, 100−113.

(7) Göbke, D.; Romanyshyn, Y.; Guimond, S.; Sturm, J. M.; Kuhlenbeck, H.; Döbler, J.; Reinhardt, U.; Ganduglia-Pirovano, M. V.; Sauer, J.; Freund, H.-J. Formaldehyde Formation on Vanadium Oxide Surfaces $V_2O_3(0001)$ and $V_2O_5(001)$: How does the Stable Methoxy Intermediate Form? *Angew. Chem., Int. Ed.* **2009**, *48*, 3695−8.

(8) Romanyshyn, Y.; Guimond, S.; Kuhlenbeck, H.; Kaya, S.; Blum, R. P.; Niehus, H.; Shaikhutdinov, S.; Simic-Milosevic, V.; Nilius, N.; Freund, H.-J.; et al. Selectivity in Methanol Oxidation as Studied on Model Systems Involving Vanadium Oxides. *Top. Catal.* **2008**, *50*, 106−115.

(9) Kresse, G.; Surnev, S.; Schoiswohl, J.; Netzer, F. P. $V_2O_3(0001)$ Surface Terminations: a Density Functional Study. *Surf. Sci.* **2004**, *555*, 118−134.

(10) Todorova, T. K.; Ganduglia-Pirovano, M. V.; Sauer, J. Vanadium Oxides on Aluminum Oxide Supports. 1. Surface Termination and Reducibility of Vanadia Films on α-$Al_2O_3(0001)$. *J. Phys. Chem. B* **2005**, *109*, 23523−31.

(11) Schoiswohl, J.; Sock, M.; Surnev, S.; Ramsey, M.; Netzer, F.; Kresse, G.; Andersen, J. $V_2O_3(0001)$ Surface Terminations: From Oxygen- to Vanadium-Rich. *Surf. Sci.* **2004**, *555*, 101−117.

(12) Dupuis, A.-C.; Abu-Haija, M.; Richter, B.; Kuhlenbeck, H.; Freund, H.-J. $V_2O_3(0001)$ on Au(111) and W(110): Growth, Termination and Electronic Structure. *Surf. Sci.* **2003**, *539*, 99−112.

(13) Kolczewski, C.; Hermann, K.; Guimond, S.; Kuhlenbeck, H.; Freund, H.-J. Identification of the Vanadyl Terminated $V_2O_3(0001)$ Surface by NEXAFS Spectroscopy: A Combined Theoretical and Experimental Study. *Surf. Sci.* **2007**, *601*, 5394−5402.

(14) Seifert, J.; Meyer, E.; Winter, H.; Kuhlenbeck, H. Surface Termination of an Ultrathin V_2O_3-film on Au(111) Studied via Ion Beam Triangulation. *Surf. Sci.* **2012**, *606*, L41−L44.

(15) Window, A.; Hentz, A.; Sheppard, D.; Parkinson, G.; Woodruff, D.; Unterberger, W.; Noakes, T.; Bailey, P.; Ganduglia-Pirovano, M.; Sauer, J. The Structure of Epitaxial V_2O_3 Films and Their Surfaces: A Medium Energy Ion Scattering Study. *Surf. Sci.* **2012**, *606*, 1716−1727.

(16) Window, A. J.; Hentz, A.; Sheppard, D. C.; Parkinson, G. S.; Niehus, H.; Ahlbehrendt, D.; Noakes, T. C. Q.; Bailey, P.; Woodruff, D. P. $V_2O_3(0001)$ Surface Termination: Phase Equilibrium. *Phys. Rev. Lett.* **2011**, *107*, 016105.

(17) Feiten, F. E.; Seifert, J.; Paier, J.; Kuhlenbeck, H.; Winter, H.; Sauer, J.; Freund, H.-J. Surface Structure of $V_2O_3(0001)$ Revisited. *Phys. Rev. Lett.* **2015**, *114*, 216101.

(18) Kröger, E. A.; Sayago, D. I.; Allegretti, F.; Knight, M. J.; Polcik, M.; Unterberger, W.; Lerotholi, T. J.; Hogan, K. A.; Lamont, C. L. A.; Woodruff, D. P. The Structure of the $V_2O_3(0001)$ Surface: A Scanned-Energy Mode Photoelectron Diffraction Study. *Surf. Sci.* **2007**, *601*, 3350−3360.

(19) Czekaj, I.; Hermann, K.; Witko, M. Ab Initio Density Functional Theory Studies on Oxygen Stabilization at the $V_2O_3(0001)$ Surface. *Surf. Sci.* **2003**, *545*, 85−98.

(20) Ascolani, H.; Cerda, J. R.; de Andres, P. L.; de Miguel, J. J.; Miranda, R.; Heinz, K. Detecting stacking faults during epitaxial growth by low energy electron diffraction. *Surf. Sci.* **1996**, *345*, 320−330.

(21) Blum, B. Single Crystal Alignment Method for LEED Experiments with Ungraded Tilt Sample-Holders. *Surf. Rev. Lett.* **1997**, *4*, 629−635.

(22) Czekaj, I.; Hermann, K.; Witko, M. Relaxation and Electronic Structure of the $V_2O_3(0001)$ Surface: Ab Initio Cluster Model Studies. *Surf. Sci.* **2003**, *525*, 33−45.

DOI: 10.1021/acs.jpcc.5b06943
J. Phys. Chem. C 2015, 119, 22961−22969

(23) Tenailleau, C.; Suard, E.; Rodriguez-Carvajal, J.; Crosnier-Lopez, M. P.; Lacorre, P. Effect of Mo Doping on the Room-Temperature Structure of Vanadium Sesquioxide. *Chem. Mater.* **2002**, *14*, 3569−3575.
(24) Igel, C.; Heidrich-Meisner, V.; Glasmachers, T. Shark. *J. Mach. Learn. Res.* **2008**, *9*, 993−996.
(25) Guimond, S.; Sturm, J. M.; Göbke, D.; Romanyshyn, Y.; Naschitzki, M.; Kuhlenbeck, H.; Freund, H.-J. Well-Ordered V_2O_5(001) Thin Films on Au(111): Growth and Thermal Stability. *J. Phys. Chem. C* **2008**, *112*, 11835−11846.
(26) van Delft, F. Bulk and Surface Debye Temperatures in Relation to Cohesive Energy and Lennard-Jones Potentials. *Surf. Sci.* **1991**, *251*−*252*, 690−695.
(27) Keer, H.; Dickerson, D.; Kuwamoto, H.; Barros, H.; Honig, J. Heat Capacity of Pure and Doped V_2O_3 Single Crystals. *J. Solid State Chem.* **1976**, *19*, 95−102.
(28) Jepsen, D. W.; Marcus, P. M.; Jona, F. The Determination of Surface Debye Temperatures from Low-Energy Electron Diffraction Data. *Surf. Sci.* **1974**, *41*, 223−236.
(29) Steurer, W.; Apfolter, A.; Koch, M.; Ernst, W. E.; Holst, B. Surface Debye Temperature of α-Quartz(0001). *Surf. Sci.* **2008**, *602*, 1080−1083.
(30) Rohr, F.; Bäumer, M.; Freund, H.-J.; Mejias, J.; Staemmler, V.; Müller, S.; Hammer, L.; Heinz, K. Strong Relaxations at the Cr_2O_3(0001) Surface as Determined via Low-Energy Electron Diffraction and Molecular Dynamics Simulations. *Surf. Sci.* **1997**, *372*, L291−L297.
(31) Lübbe, M.; Moritz, W. A LEED Analysis of the Clean Surfaces of α-Fe_2O_3(0001) and α-Cr_2O_3(0001) Bulk Single Crystals. *J. Phys.: Condens. Matter* **2009**, *21*, 134010.
(32) Ketteler, G.; Weiss, W.; Ranke, W. Surface Structures of α-Fe_2O_3(0001) Phases Determined by LEED Crystallography. *Surf. Rev. Lett.* **2001**, *8*, 661−683.
(33) Rehbein, C.; Harrison, N.; Wander, A. Structure of the α-Cr_2O_3(0001) Surface: An Ab Initio Total-Energy Study. *Phys. Rev. B: Condens. Matter Mater. Phys.* **1996**, *54*, 14066−14070.
(34) Rohrbach, A.; Hafner, J.; Kresse, G. Ab Initio Study of the (0001) Surfaces of Hematite and Chromia: Influence of Strong Electronic Correlations. *Phys. Rev. B: Condens. Matter Mater. Phys.* **2004**, *70*, 1−17.
(35) Bergermayer, W.; Schweiger, H.; Wimmer, E. Ab Initio Thermodynamics of Oxide Surfaces: O_2 on Fe_2O_3(0001). *Phys. Rev. B: Condens. Matter Mater. Phys.* **2004**, *69*, 1−12.
(36) Niehus, H.; Blum, R.-P.; Ahlbehrendt, D. Structure of Vanadium Oxide (V_2O_3) Grown on Cu_3Au(100). *Surf. Rev. Lett.* **2003**, *10*, 353−359.
(37) Surnev, S.; Kresse, G.; Sock, M.; Ramsey, M. G.; Netzer, F. P. Surface Structures of Ultrathin Vanadium Oxide Films on Pd(111). *Surf. Sci.* **2001**, *495*, 91−106.
(38) Walters, C. F.; Mccarty, K. F.; Soares, E. A.; Van Hove, M. A. The Surface Structure of α-Al_2O_3 Determined by Low-Energy Electron Diffraction: Aluminum Termination and Evidence for Anomolously Large Thermal Vibrations. *Surf. Sci.* **2000**, *464*, L732−L738.
(39) Seifert, J.; Busch, M.; Meyer, E.; Winter, H. Surface Structure of Alanine on Cu(110) via Grazing Scattering of Fast Atoms and Molecules. *Phys. Rev. B: Condens. Matter Mater. Phys.* **2014**, *89*, 075404.

DOI: 10.1021/acs.jpcc.5b06943
J. Phys. Chem. C 2015, 119, 22961−22969